NASA TECHNICAL NOTE

NASA TN D-5359

NASA TN D-5359

FLIGHT MEASUREMENTS OF CANARD LOADS, CANARD BUFFETING, AND ELEVON AND WING-TIP HINGE MOMENTS ON THE XB-70 AIRCRAFT INCLUDING COMPARISONS WITH PREDICTIONS

by Jerald M. Jenkins, V. Michael DeAngelis, Edward L. Friend, and Richard C. Monaghan

Flight Research Center
Edwards, Calif.

NATIONAL AERONAUTICS AND SPACE ADMINISTRATION • WASHINGTON, D. C. • AUGUST 1969

TECHNICAL REPORT STANDARD TITLE PAGE

1. Report No. NASA TN D-5359	**2. Government Accession No.**	**3. Recipient's Catalog No.**
4. Title and Subtitle FLIGHT MEASUREMENTS OF CANARD LOADS, CANARD BUFFETING, AND ELEVON AND WING-TIP HINGE MOMENTS ON THE XB-70 AIRCRAFT INCLUDING COMPARISONS WITH PREDICTIONS		**5. Report Date** August 1969 **6. Performing Organization Code**
7. Author(s) Jerald M. Jenkins, V. Michael DeAngelis, Edward L. Friend, and Richard C. Monaghan		**8. Performing Organization Report No.** H-554
9. Performing Organization Name and Address NASA Flight Research Center P. O. Box 273 Edwards, Calif. 93523		**10. Work Unit No.** 720-51-00-04-24 **11. Contract or Grant No.**
12. Sponsoring Agency Name and Address National Aeronautics and Space Administration Washington, D. C. 20546		**13. Type of Report and Period Covered** Technical Note **14. Sponsoring Agency Code**

15. Supplementary Notes

16. Abstract

Flight-test data are presented from Mach 0.40 to Mach 3.00. The data are compared with the manufacturer's rigid and aeroelastic predictions, wind-tunnel airfoil data, or results derived from flight tests of other comparable aircraft.

17. Key Words Suggested by Author(s) XB-70 airplane - Flight loads - Buffeting	**18. Distribution Statement** Unclassified - Unlimited

19. Security Classif. (of this report) Unclassified	**20. Security Classif. (of this page)** Unclassified	**21. No. of Pages** 28	**22. Price** $3.00

FLIGHT MEASUREMENTS OF CANARD LOADS, CANARD BUFFETING, AND ELEVON AND WING-TIP HINGE MOMENTS ON THE XB-70 AIRCRAFT INCLUDING COMPARISONS WITH PREDICTIONS

By Jerald M. Jenkins, V. Michael DeAngelis,
Edward L. Friend, and Richard C. Monaghan
Flight Research Center

SUMMARY

During a flight-test program with the XB-70 airplane, canard, elevon, and wing-tip flight load measurements were made in the Mach number range from 0.40 to 3.00. The data are compared with the manufacturer's rigid and aeroelastic predictions, wind-tunnel airfoil data, or results obtained from flight tests of other applicable aircraft.

The magnitudes of the flight loads and the variation of surface loads with angle of attack or surface deflection corresponded generally with predictions. Canard buffeting was experienced at subsonic speeds. The characteristics of this effect are examined on the basis of the results of in-flight tuft studies and the analysis of flight-measured bending-moment data.

INTRODUCTION

In the design and construction of a new high-performance airplane, considerable savings can be effected by verifying existing design/predictive techniques with flight results on a comparable configuration. This validation is particularly important when considering large and expensive aeroflexible vehicles such as future supersonic transports, whose economic feasibility depends to such an extent on aerodynamic, structural, operational, and performance predictions. To obtain pertinent data on large-airplane characteristics as well as to check on existing predictive techniques, the XB-70 airplanes were used in a program directed toward the investigation of the general flight characteristics of a large high-performance airplane. Some of the data resulting from these studies are reported in references 1 to 7.

As a part of these studies with the XB-70 airplane, strain-gage load measurements were made on the canard, folding wing tips, and elevons during flight tests; the results are reported herein. Since the correlation of flight load measurements on the lifting and control surfaces with design information is a basic requirement for ascertaining the general structural integrity of a newly developed aircraft, such correlations are presented in this report. The XB-70 flight data are compared with rigid wind-tunnel-model data, aeroelastic predictions, wind-tunnel airfoil data, and results from flight

tests of other aircraft. In addition, flight data defining the buffeting characteristics of the canard are documented.

SYMBOLS

Measurements were taken in the U.S. Customary System of Units. Equivalent units in the International System of Units are provided. Details concerning the use of SI, together with physical constants and conversions, are given in reference 8.

B_c canard-panel aerodynamic root bending moment, inch-pounds (meter-newtons)

$\frac{b_c}{2}$ semispan of the exposed canard panel, 125.5 in. (3.19 m), inches (meters)

$\frac{b_t}{2}$ semispan of wing tip outboard of hinge line, 20.78 ft (6.33 m), feet (meters)

C_{B_c} canard bending-moment coefficient, $\frac{B_c}{qS_c\left(\frac{b_c}{2}\right)}$

C_{h_e} elevon-segment hinge-moment coefficient, $\frac{HM_e}{qS_e\bar{c}_e}$

$\bar{C}_{h_e}$ average elevon hinge-moment coefficient, $\frac{\overline{HM}_e}{q\bar{S}_e\bar{c}_e}$

C_{h_t} wing-tip hinge-moment coefficient, $\frac{HM_t}{qS_t\left(\frac{b_t}{2}\right)}$

$C_{h_{\delta_e}} = \frac{\partial C_{h_e}}{\partial \delta_e}$, per degree

$\bar{C}_{h_{\bar{\delta}_e}} = \frac{\partial \bar{C}_{h_e}}{\partial \bar{\delta}_e}$, per degree

C_{N_c} canard normal-force coefficient, $\frac{V_c}{qS_c}$

$C_{N_{\alpha_c}} = \frac{\partial C_{N_c}}{\partial \alpha_c}$, per degree

C_{T_c} canard torsional-moment coefficient, $\frac{T_c}{qS_c\bar{c}_c}$

$\bar{c}_c$ mean aerodynamic chord of the exposed canard panel, 158.91 in. (4.04 m), inches (meters)

$\bar{c}_e$ average elevon chord, 116.0 in. (2.95 m), inches (meters)

HM_e individual elevon-segment aerodynamic hinge moment, inch-pounds (meter-newtons)

$\overline{HM}_e$ average elevon aerodynamic hinge moment, inch-pounds (meter-newtons)

HM_t wing-tip aerodynamic hinge moment, inch-pounds (meter-newtons)

h_p altitude, feet (meters)

M Mach number

q free-stream dynamic pressure, pounds/foot^2 (newtons/meter^2)

q_{ref} reference free-stream dynamic pressure used for normalizing unsteady bending-moment data, 300 lb/ft^2 (14,360 N/m^2), pounds/foot^2 (newtons/meter^2)

S_c exposed panel area of one surface of the canard, 132.64 ft^2 (12.32 m^2), feet^2 (meters^2)

S_e individual elevon-segment area, feet^2 (meters^2)

$\bar{S}_e$ — average elevon area, 32.95 ft^2 (3.06 m^2), $feet^2$ ($meters^2$)

S_t — area of wing tip outboard of hinge line, 520.90 ft^2 (48.39 m^2), $feet^2$ ($meters^2$)

T_c — canard-panel aerodynamic root torsion, inch-pounds (meter-newtons)

V_c — canard-panel aerodynamic root shear, pounds (newtons)

x_{cp} — canard chordwise center-of-pressure location measured from the leading edge of the exposed mean aerodynamic chord, inches (meters)

$\frac{x_{cp}}{\bar{c}_c}$ — canard chordwise center of pressure of the additional load, $\frac{\partial C_{T_c}}{\partial C_{N_c}}$, fraction of mean aerodynamic chord of exposed canard panel

y_{cp} — canard spanwise center-of-pressure location measured from the canard root rib, inches (meters)

$\frac{2y_{cp}}{b_c}$ — canard spanwise center of pressure of the additional load, $\frac{\partial C_{B_c}}{\partial C_{N_c}}$, fraction of span of exposed canard panel

α — airplane angle of attack, degrees

α_c — canard angle of attack, $\alpha + \delta_c$, degrees

δ_c — canard deflection, degrees

δ_e — elevon-segment deflection, degrees

$\bar{\delta}_e$ — average elevon deflection, degrees

δ_t — wing-tip deflection measured from fuselage reference plane, degrees

σ_B root-mean-square unsteady bending moment, inch-pounds (meter-newtons)

$\bar{\sigma}_B$ normalized root-mean-square unsteady bending moment, $\frac{\sigma_B}{\sqrt{\frac{q}{q_{ref}}}}$, inch-pounds (meter-newtons)

Φ_B unsteady bending-moment power spectral density, $\frac{(\text{inch-pounds})^2}{\text{cycles per second}}$ $\left(\frac{(\text{meter-newtons})^2}{\text{cycles per second}}\right)$

AIRCRAFT

The XB-70 airplane (see fig. 1), originally designed as a long-range supersonic bomber, has a thin, low-aspect-ratio, highly swept delta wing with folding wing tips, twin movable vertical stabilizers, elevon surfaces for pitch and roll control, a movable canard with trailing-edge flaps, and twin inlets enclosed in a single nacelle. Two vehicles were built and were identical in configuration except that the first (XB-70-1) had zero geometric dihedral, and the second (XB-70-2) had 5° geometric dihedral. The airplane has a design gross weight in excess of 500,000 pounds (220,800 kilograms) and a design cruising speed of Mach 3.0 at approximately 70,000 feet (21,300 meters) altitude.

E-16694

Figure 1.– XB-70 airplane.

The elevons are segmented, with six segments on each wing semispan (see fig. 2).

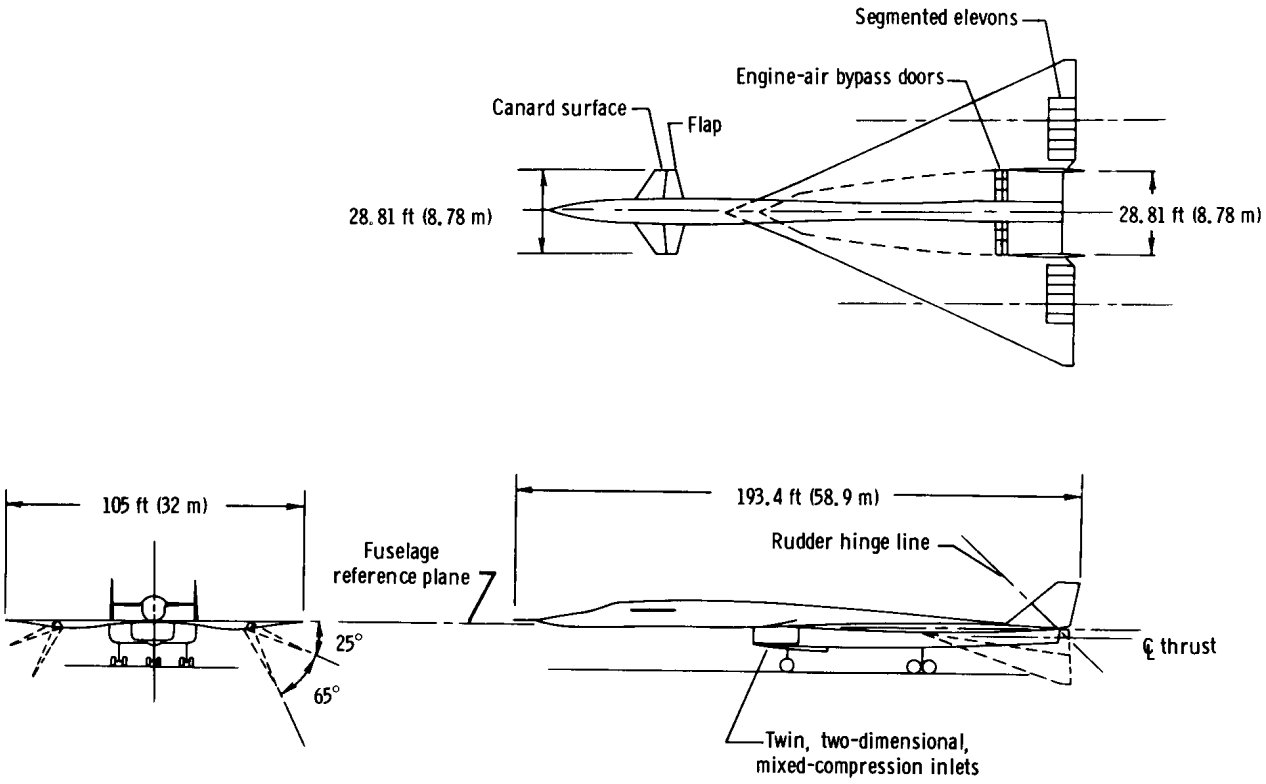

Figure 2.– Three-view drawing of XB-70-1 airplane.

Each segment is hinged at the top surface and is deflected by two actuators attached near the bottom surface. The elevon control system is irreversible and hydraulically actuated. A common signal commands the hydraulic actuators. The elevon deflection is directly coordinated with the canard during normal flight to provide longitudinal control. During landings and takeoffs the canard position is fixed, the canard flaps are fully deflected 20°, and the elevons provide the only longitudinal control. The two outboard elevon segments on each wing panel are on the folding wing tips. When the wing tips are folded down (at 25° or 65°, depending upon the flight condition), the two outboard segments fold with the wing tip, are fixed at zero deflection, and are not used for control. The wing tips are usually flown at zero deflection up to approximately Mach 0.8; beyond that the wing tips must be folded and, consequently, only eight elevon segments are available for control.

In the normal flight configuration, longitudinal control is obtained from the canard and elevons with the canard flap undeflected. When the flight augmentation control system is not in use, the canard and elevon deflections are linearly related (ref. 6).

Both canard surfaces deflect simultaneously; there are no aileron capabilities from the canard.

The geometric characteristics of the airplane, including the exposed canard panel, are presented in table I. Additional information concerning the operation, stability and control, propulsion, and general characteristics of the XB-70 airplanes is presented in references 6 and 1.

INSTRUMENTATION

Strain Gages

Canard. – The right and left canard surfaces are joined by a carry-through structure which attaches to the root rib of each surface. Each canard surface is joined to the fuselage by a universal pivot point at the rear of the root rib. It is deflected by using an actuator attached to the front of the root rib. The canard is instrumented to measure root bending moment, root shear, and root torque for both the right and left surfaces. The bending moment is measured by four bending bridges mounted on each side of the carry-through structure slightly inboard from the root rib. The shear load of each panel is obtained from three shear bridges, a bending bridge, and the canard actuator load for the particular panel, and the left and right canard-surface bending-moment equations. The shear bridges are near the canard attachment point on the root rib, the aft beam of the main box, and the aft beam of the carry-through structure. The bending bridge is located on the last cell of the carry-through structure and is also used for measuring bending moment. The torque is computed about the canard attachment point from the canard actuator load, sensed by linear-axial-force-sensing gages.

Elevons. – Elevon hinge moments are obtained by measuring actuator loads with strain gages in a conventional linear-axial-force-sensing manner. Loads data were obtained on eight of the twelve elevon segments. All six segments on the right side and two segments on the left side were instrumented. The segments are numbered starting with the first inboard segment as 1 and progressing to the last outboard segment, designated 6. Elevon segments 1 and 4 were instrumented on the left side.

Wing tips. – The folding wing tips are hinged to the primary wing structure at six attachment points on each wing. The wing tips are flown at three deflected positions: 0°, 25°, and 65°. Each wing tip is instrumented for hinge-moment measurements. The total hinge moment of each wing tip is obtained by summing the hinge moments of all six actuators which are instrumented with strain gages.

Aircraft Parameters

Flight data were obtained with a pulse code modulation (PCM) data-acquisition system. Approximately 1100 parameters were recorded during each flight to obtain data on several concurrent programs. The PCM system converts analog signals from the sensor to digital format and records the digitized data on tape on a time-sharing basis. The flight parameters used in analyzing loads data were the same as those used in the study of reference 6, in which the sensor characteristics and accuracies are tabulated.

FLIGHT-TEST DATA

Flight-Test Conditions

The altitude and Mach number conditions at which flight-test data were acquired are presented in figure 3. Most of the flight data was obtained during either level flight, wind-up turns, or push-over/pullup maneuvers. Flight loads data were measured on both test aircraft; however, most of the data was obtained on the XB-70-2. The specific flight conditions at which data were acquired are presented in table II.

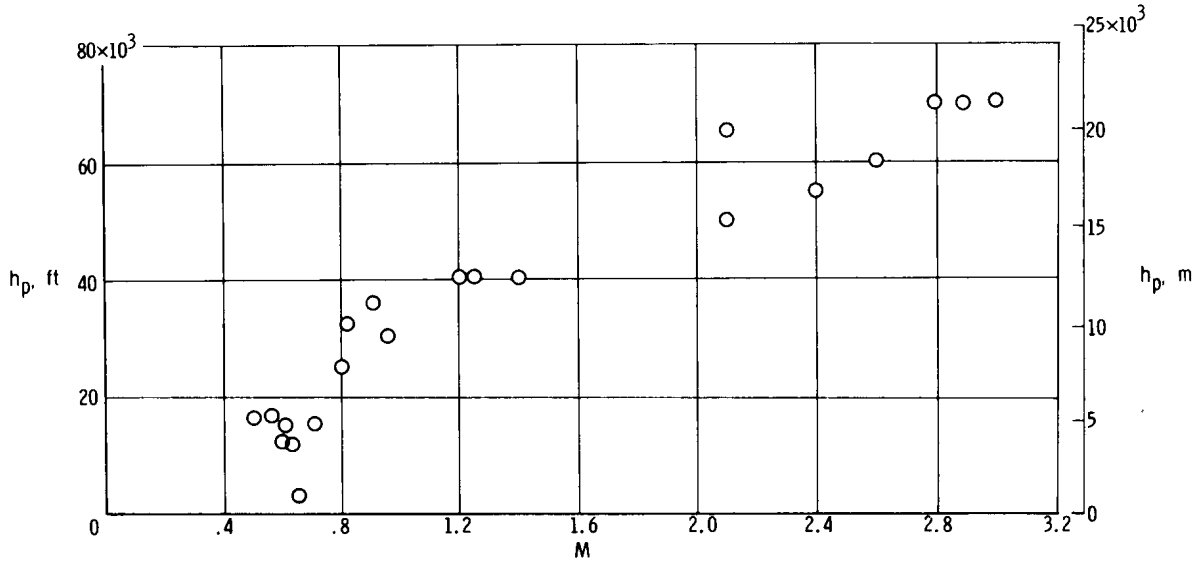

Figure 3.– Flight conditions for XB-70 loads data.

Data Analysis

The outputs of the lifting- and control-surface strain-gage bridges as well as basic aircraft parameters were recorded during flight-test maneuvers utilizing the data-acquisition system discussed in the Aircraft Parameters section. The data were then fed into a ground-based computer in which the mathematical equations defining the basic aircraft parameters and the relationship between the strain-gage-bridge outputs and the applied structural load were stored. These mathematical relationships were established before the flight tests by conventional ground load calibration techniques (ref. 9). Tabulated and plotted flight loads data and aircraft parameters were obtained from the computer. Selected data points were then chosen, and the loads data were reduced to aerodynamic load coefficient form.

The pertinent force, hinge moment, and deflection sign conventions used in the data analysis are shown in figure 4.

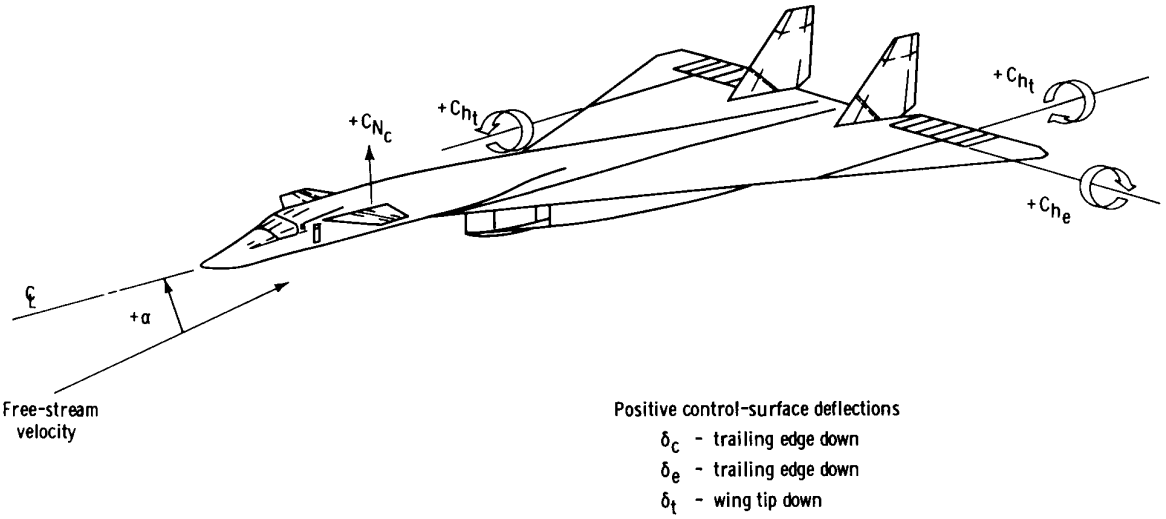

Figure 4.– Sign conventions.

PREDICTIONS AND WIND-TUNNEL DATA

Both the rigid and the aeroelastic predictions of the canard loads and elevon hinge moments were made by the manufacturer. The rigid loads predictions, contained in reference 10, were based upon rigid-model wind-tunnel tests in numerous facilities. The aeroelastic loads predictions (previously unpublished) were obtained from the static aeroelastic predictions for the complete vehicle, which were calculated by using a direct-influence coefficient technique.

Additional information from the results of specific wind-tunnel tests is provided for comparison purposes. The rigid-model wind-tunnel data for the wing-tip hinge moments were obtained by integrating the rigid-model pressure data of reference 11. Supersonic elevon hinge-moment data were obtained directly from reference 12, since the model was constructed with a segmented elevon. The model upon which the predictions of reference 10 were based was constructed with an unsegmented (slab) elevon.

RESULTS AND DISCUSSION

Canard Loads

Canard root shear loads measured during maneuvering flight are presented in normal-force-coefficient form in figure 5. The normal-force-coefficient values are

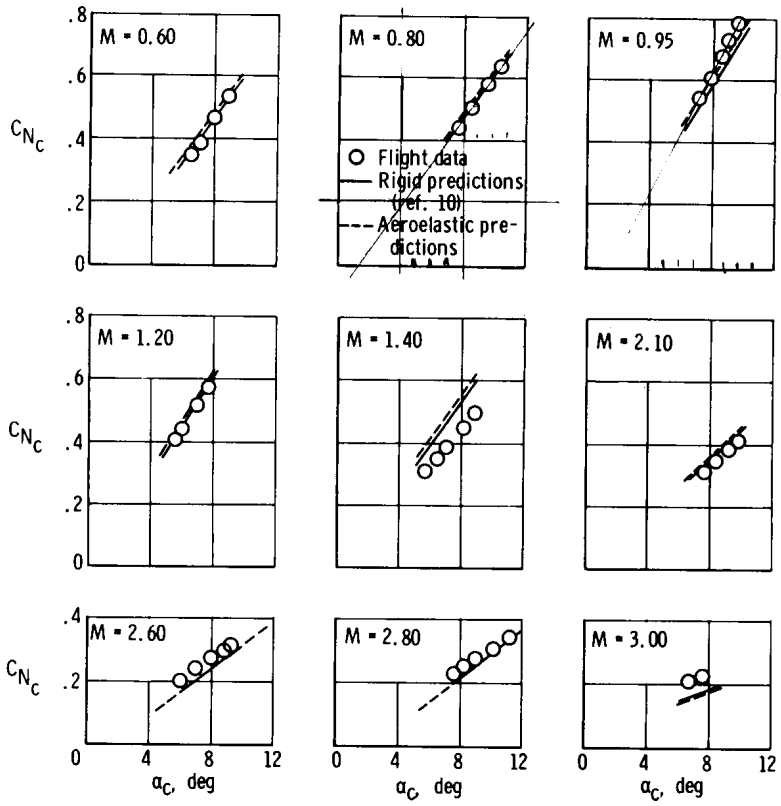

Figure 5.– Comparison of canard normal-force-coefficient data with predicted values.

plotted versus canard angle of attack for Mach numbers from 0.60 to 3.00. The flight data are compared with both rigid and aeroelastic predictions. The predicted values agree closely with flight data at subsonic and transonic speeds. The flight data are approximately 0.1 normal-force coefficient less than the predictions at Mach 1.40 and approximately 0.1 larger than the predictions at Mach 3.00. The general correlation of canard flight data with the predicted values of figure 5 indicates no large variations or unusual occurrences. However, the flight tests were not conducted at widely varying or significantly large free-stream dynamic pressure; hence, the aeroelastic effects can be assessed only for the specific data presented. It should be noted that the normal-force-coefficient data of figure 5 are plotted against the canard angle of attack, which is the sum of the airplane angle of attack and the canard deflection. The flight data and predictions presented account for the specific proportions of canard deflections and aircraft angle of attack; however, the results should not be extrapolated to other combinations of canard deflection and aircraft angle of attack.

Values of the slopes of canard normal-force coefficient versus canard angle of attack are presented in figure 6 for most of the test conditions. The flight-determined $C_{N_{\alpha_c}}$ values are slightly larger than predictions at subsonic speeds and slightly smaller than predictions at supersonic speeds. The single flight-determined transonic point is significantly larger than predicted values. The $C_{N_{\alpha_c}}$ slopes are also compared with data from other aircraft having wing—fuselage planforms similar to the canard—fuselage

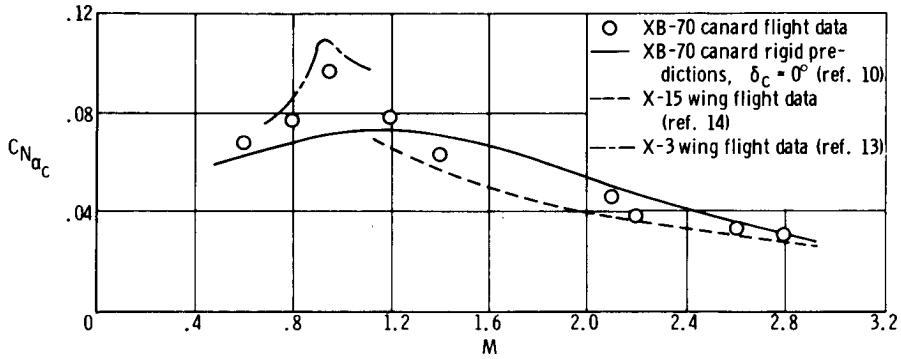

Figure 6.– Variation of flight-determined XB-70 canard normal-force-coefficient slopes with Mach number and comparison with predicted values for XB-70 canard and with flight results of other aircraft.

planform of the XB-70. Subsonically and transonically, the canard data are compared with data acquired on the wing of the X-3 airplane (ref. 13); supersonically, they are compared with data obtained on the wing of the X-15 airplane (ref. 14). The XB-70 flight data compare generally well with the predicted values and the results from the other aircraft.

In addition to the canard shear loads, the root bending moment and torque were measured during the maneuvering flight tests. These three measurements provided sufficient information to determine the spanwise and chordwise center-of-pressure locations of the additional airload. The resulting center-of-pressure locations are presented in figure 7 and compared with predicted locations. The flight-determined

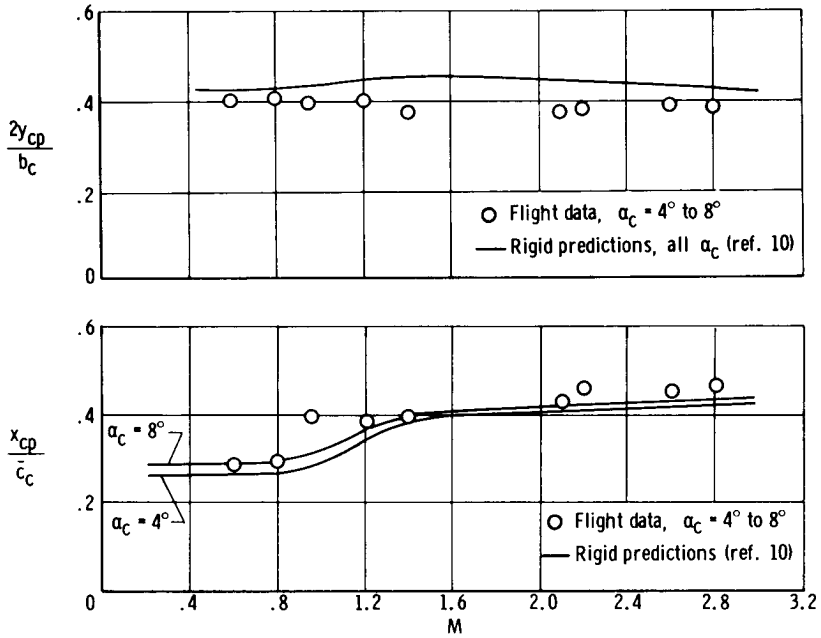

Figure 7.– Variation of flight-determined canard center-of-pressure location of the additional airload with Mach number and comparison with predicted values.

spanwise center-of-pressure location agrees closely with predictions at subsonic speeds; however, at transonic and low supersonic speeds, it is considerably inboard of predictions. At the higher supersonic speeds, the flight-determined spanwise center of pressure corresponds more closely to predictions. The chordwise center-of-pressure location of the additional airload measured in flight is somewhat aft of the predictions at supersonic speeds. At subsonic speeds the agreement with predictions is generally good. The transonic flight-determined chordwise center of pressure, at Mach 0.95, is considerably aft of the predictions.

Canard Buffeting

Early in the XB-70 flight-test program, an unsteady force input was noticed subsonically in the extreme forward area of the aircraft. Tufting of the canard upper surface revealed that a leading-edge flow separation was occurring in that area. The tuft behavior was examined photographically. The flow separation on the upper surface of the canard is depicted in figure 8. At Mach 0.4 and an angle of attack of 10° (fig. 8(a)), the tufts revealed a large area of reverse flow and essentially no steady aft flow anywhere on the upper surface. At Mach 0.6 and an angle of attack of 6° (fig. 8(b)), a smaller area of reverse flow was revealed, and a region of steady aft flow was noted. At Mach 0.9 and an angle of attack of 4° (fig. 8(c)), only a small area of unsteady aft flow was noticed, with most of the upper surface flow being steady aft.

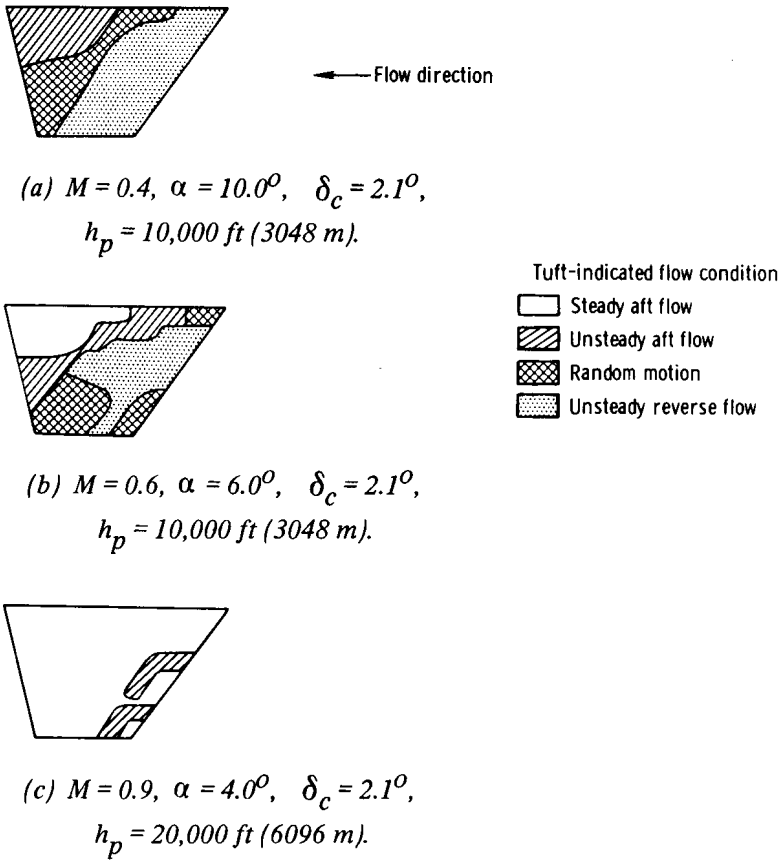

(a) $M = 0.4$, $\alpha = 10.0^{o}$, $\delta_c = 2.1^{o}$, $h_p = 10{,}000$ ft (3048 m).

(b) $M = 0.6$, $\alpha = 6.0^{o}$, $\delta_c = 2.1^{o}$, $h_p = 10{,}000$ ft (3048 m).

(c) $M = 0.9$, $\alpha = 4.0^{o}$, $\delta_c = 2.1^{o}$, $h_p = 20{,}000$ ft (6096 m).

Figure 8.– Flow conditions on the upper canard surface as determined from in-flight tuft tests.

Once the source of the unsteady forces was identified clearly as the canard surface, additional data were acquired by utilizing the strain-gage load-measuring capabilities of the canard. Canard root bending moment was measured during six special push-over/pullup maneuvers. These measurements provided unsteady bending-moment data over a wide range of angle of attack. Root-mean-square values of the unsteady bending moment were calculated, normalized to a reference free-stream dynamic pressure, and plotted versus canard angle of attack, as shown in figure 9. The root-mean-square values of unsteady bending moment were normalized to the square root of

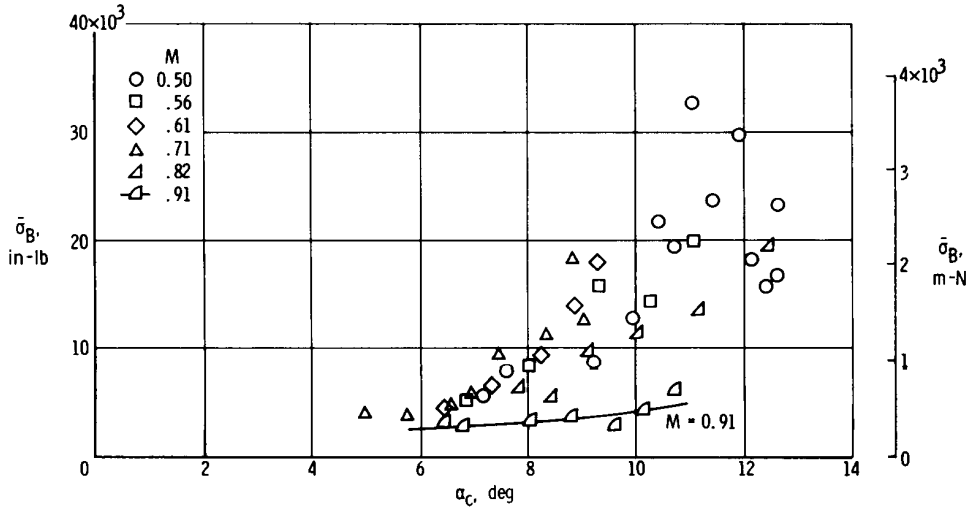

Figure 9.– Variation of canard unsteady bending moment normalized to 300 lb/ft^2 (14,360 N/m^2) with canard angle of attack for several Mach numbers.

the free-stream dynamic-pressure ratio through the relationship:

$$\bar{\sigma}_B = \frac{\sigma_B}{\sqrt{\frac{q}{q_{ref}}}}$$

Normalizing flight buffet data at varying flight conditions is discussed in references 15 and 16. The normalized data presented in figure 9 indicate a clear reduction in the magnitude of unsteady bending moment as the transonic region is approached. A line was faired through the Mach 0.91 data to illustrate this point.

A similar type of flow problem was experienced in the flight-test program on the wing of the X-3 airplane (ref. 17), which had a thin modified hexagonal profile airfoil like the XB-70 canard. Similar results were noted on a 4-percent-thick, two-dimensional airfoil tested in a wind tunnel (ref. 18). These wind-tunnel tests indicated a reduction of unsteady forces as the transonic region was approached.

Although the magnitude of the unsteady bending moment became large subsonically, no appreciable loss of lift occurred on the canard panel. The normal-force coefficient is plotted against canard angle of attack in figure 10 for the two Mach numbers at which

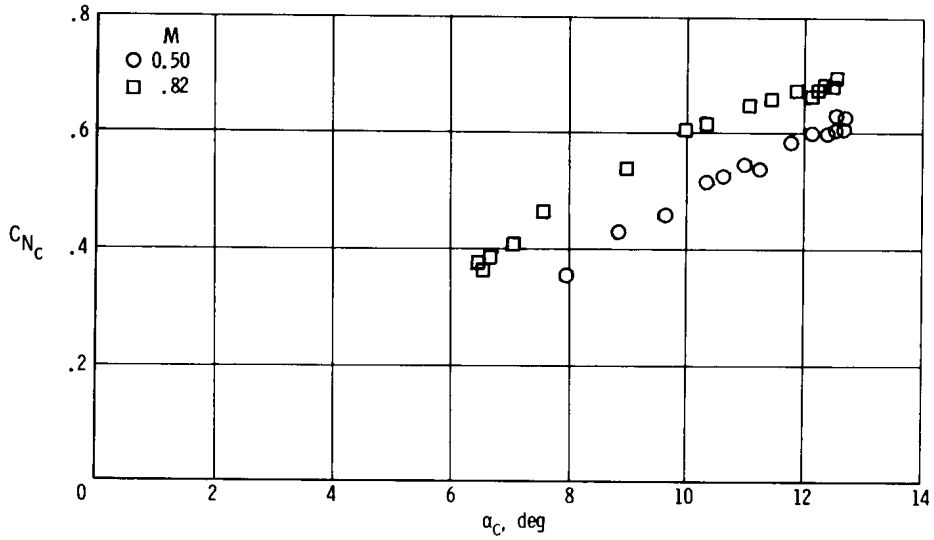

Figure 10.– Variation of canard panel normal-force-coefficient with canard angle of attack.

the largest angle of attack was reached. The Mach 0.50 condition indicates only a very small change in slope with increase in canard angles of attack. However, as shown in the data of figure 9, the unsteady bending moments appear to be quite large at the higher angles of attack. The Mach 0.82 test condition shows a reduction in slope at an angle of attack of about 10°, but the change is still small through 12° angle of attack. The corresponding root-mean-square bending-moment data (fig. 9) indicate that the unsteady bending moments are continually increasing as the angle of attack increases. The other four test conditions provided identical trends, in that little or no apparent loss of lift occurred with increasing angle of attack.

The movement of the center of pressure of the additional load was also examined for the six buffet test conditions. The spanwise center of pressure was found to move somewhat inboard as the canard angle of attack increased, and the chordwise center of pressure moved aft as the canard angle of attack increased. Typical results are presented in figure 11 for the Mach 0.50 and 0.82 buffeting conditions. The resultant

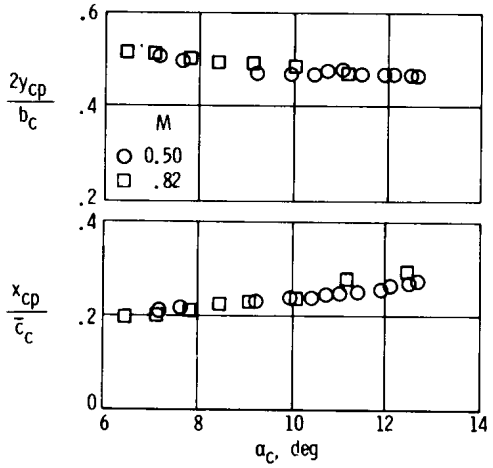

Figure 11.– Canard center-of-pressure variations during buffeting conditions.

center-of-pressure movements corresponded with the results of the tuft study which indicated that the separated flow condition was most severe in the forward and outboard areas of the canard.

The gradual manner in which the canard center of pressure of the additional load changed explains the absence of an abrupt canard normal-force break during angle-of-attack increases. The separated flow region is thought to be continually increasing in size as the angle of attack is increased. This would result in a proportionate loss of normal force with increasing angle of attack, which would not appear as an abrupt break in the normal force but would be observed as a general reduction of the overall normal-force-coefficient slope with increasing angle of attack. Hence, if the flow separation were not occurring, the variation in canard normal-force coefficient with angle of attack would have a steeper slope.

To complete the analysis of the unsteady canard loads, two typical power-spectral-density plots are presented in figure 12 for the test conditions shown in figure 10. The plots indicate the predominant frequency to be at approximately 9 cycles per second for both Mach numbers. This frequency corresponds closely to the canard first bending frequency established in ground vibration tests. A small amount of power exists at a higher, secondary frequency (approximately 14 cps); however, most of the energy enters the fuselage structure by way of the canard first bending mode.

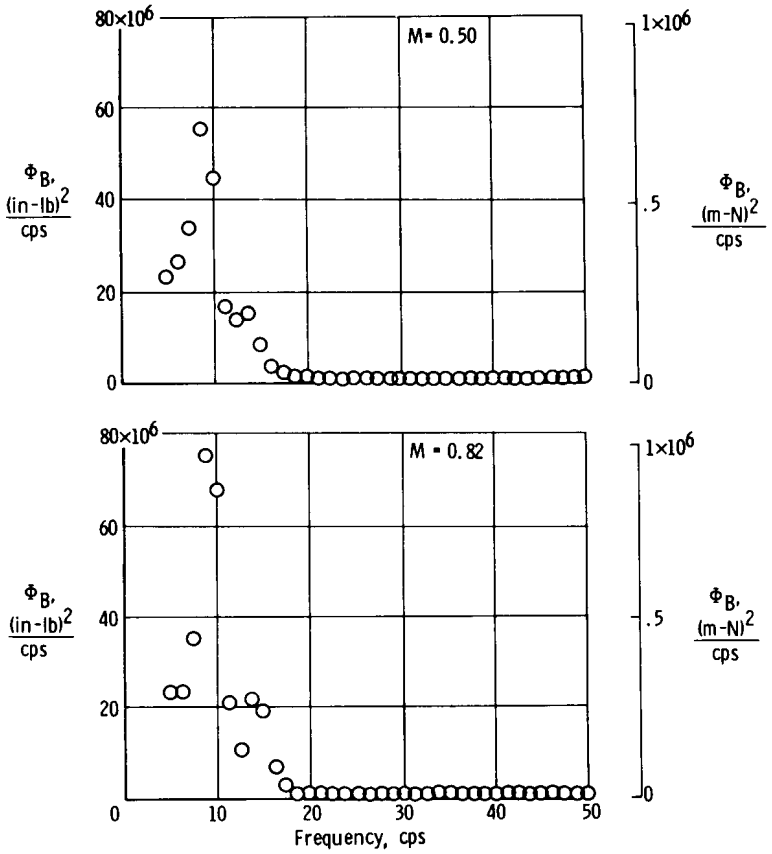

Figure 12.– Power spectral density of the canard-panel bending moment.

Elevon Hinge Moments

Elevon hinge-moment data are presented in figures 13 to 15 in the form of average elevon hinge-moment coefficients. All the elevon data were acquired on the XB-70-2 airplane. This coefficient is determined by summing the total hinge moments of all the right-wing elevon segments and dividing by the total right-wing elevon area and average elevon chord. The flight data are plotted against average elevon deflection, which is the sum of all right-wing elevon-segment deflections divided by the number of right-wing segments in use. Data are presented in figure 13 for two subsonic Mach numbers and zero wing-tip deflection. The flight data are presented for specific angles of attack and are compared with predictions. In the top plot the flight data agree closely with rigid and aeroelastic predictions. No aeroelastic predictions were available for comparison with the flight data in the lower plot; however, the flight data generally agree closely with the rigid predictions which were available.

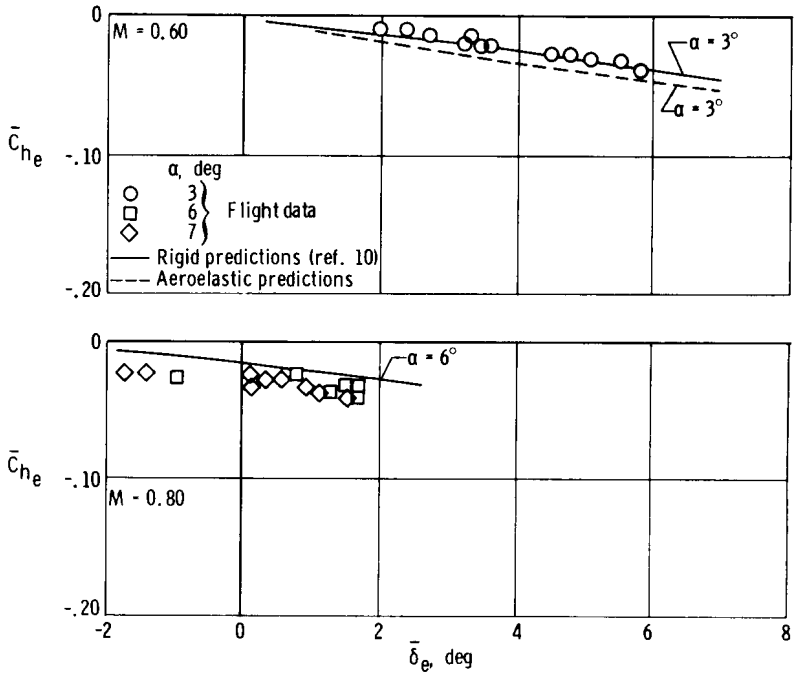

Figure 13.– Comparison of flight-measured average elevon hinge-moment-coefficient data with predicted values at $\delta_t = 0^o$.

Elevon data for the 25° wing-tip deflection are presented in figure 14 for Mach numbers from 0.65 to 1.40. The subsonic flight data at Mach 0.65 and 0.80 agree closely with predictions. The transonic levels of $\bar{C}_{h_e}$ are significantly less than rigid predictions, but agree closely with aeroelastic predictions. At Mach 1.25 the magnitudes of the flight data are significantly less than the rigid predictions and somewhat less than the aeroelastic predictions. At Mach 1.40 the levels of the flight data are less than the rigid predictions, but agree fairly closely with the aeroelastic predictions.

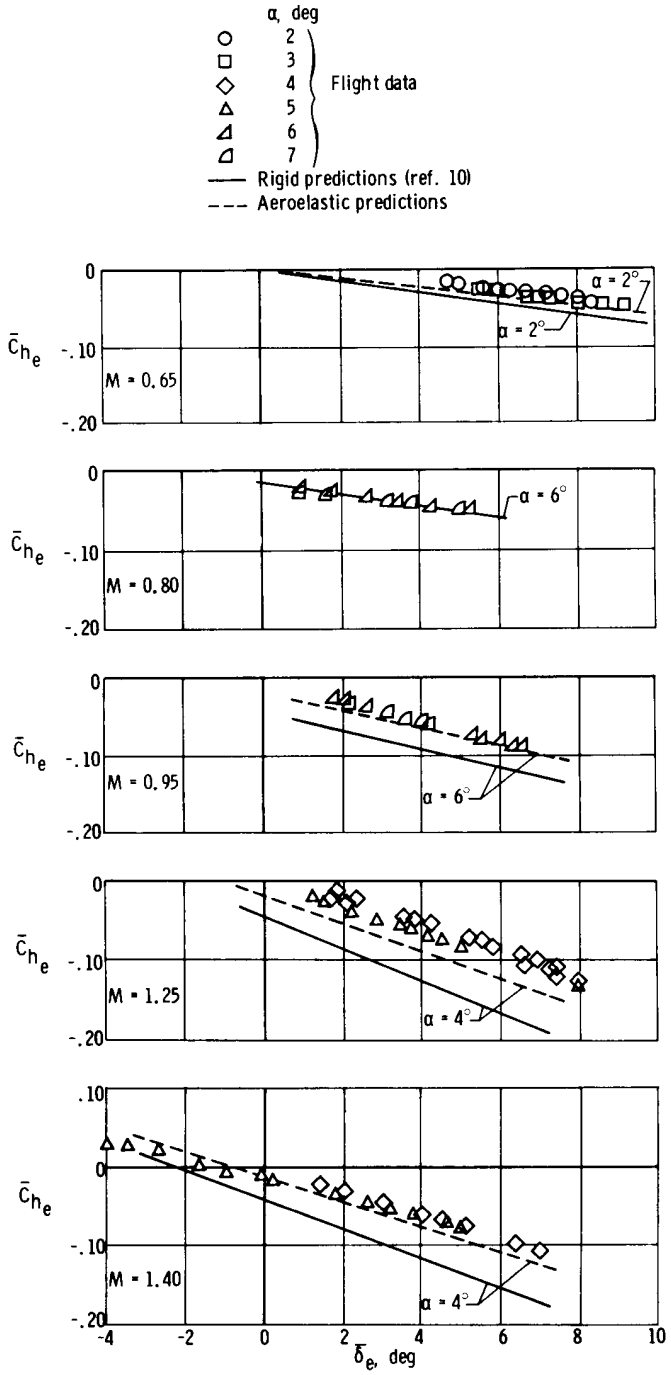

Figure 14.– Comparison of flight-measured average elevon hinge-moment-coefficient data with predicted values at $\delta_t = 25^o$.

The elevon data for the 65° wing-tip deflection are presented in figure 15 for Mach numbers from 1.20 to 3.00. The levels of the flight data at Mach 1.20 and 1.40 are significantly less than the rigid predictions and slightly less than the aeroelastic predictions. At Mach 2.10 the magnitudes of the flight data are somewhat larger than the

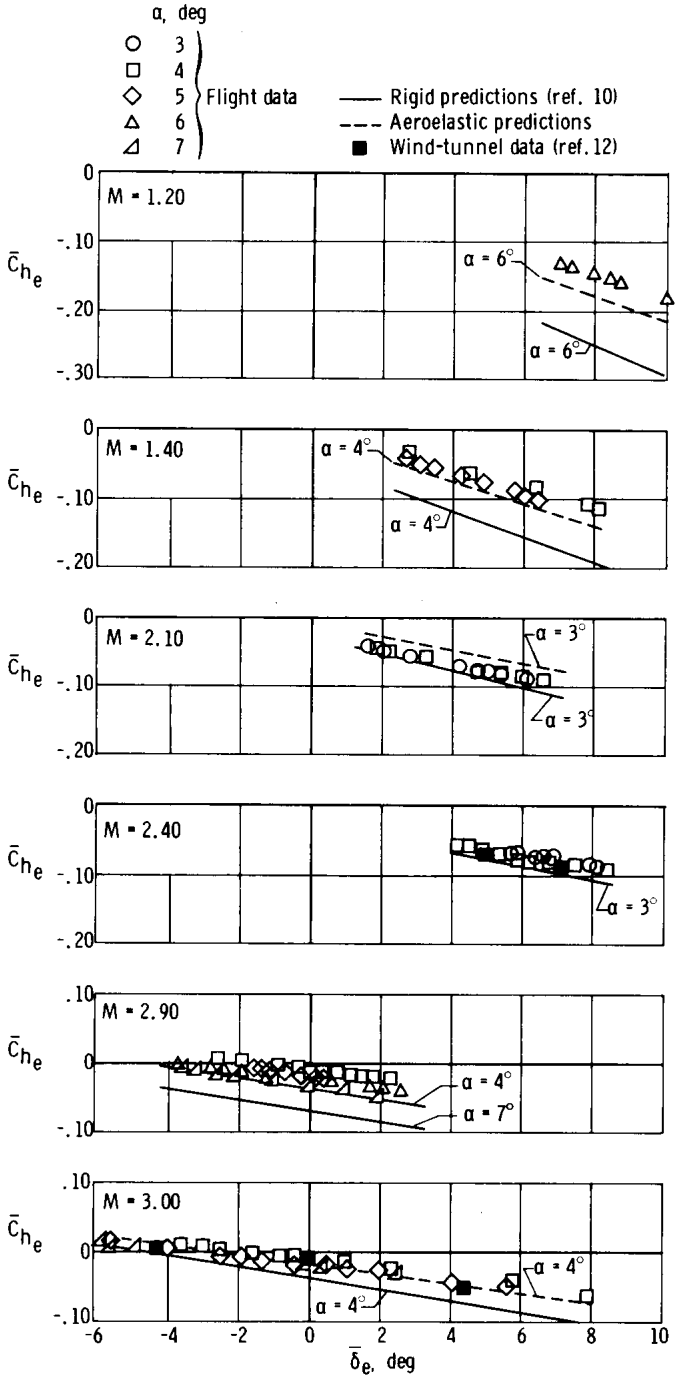

Figure 15.– Comparison of flight-measured average elevon hinge-moment-coefficient data with predicted values at $\delta_t = 65^o$.

aeroelastic predictions and slightly smaller than the rigid predictions. No aeroelastic predictions were available at Mach 2.40, but the levels of the flight data are slightly less than rigid predictions and agree closely with the wind-tunnel data of reference 12. At Mach 2.90 the magnitudes of the flight data are somewhat smaller than the rigid predictions. The levels of the flight data at Mach 3.00 are somewhat less than rigid predictions, but agree well with the aeroelastic predictions and the wind-tunnel data of reference 12.

In general, the elevon hinge-moment-coefficient flight data agreed well with predictions and wind-tunnel data. The most significant deviations were in and near the higher transonic region.

The slopes of the curves of average elevon hinge-moment coefficient with average elevon deflection, as a function of Mach number, are presented in figure 16 for Mach numbers from 0.60 to 3.00 for the three basic wing-tip positions. The flight data are compared with rigid and aeroelastic predictions. The overall comparison of the flight data with predictions indicates either close correlation or slightly lower slopes than

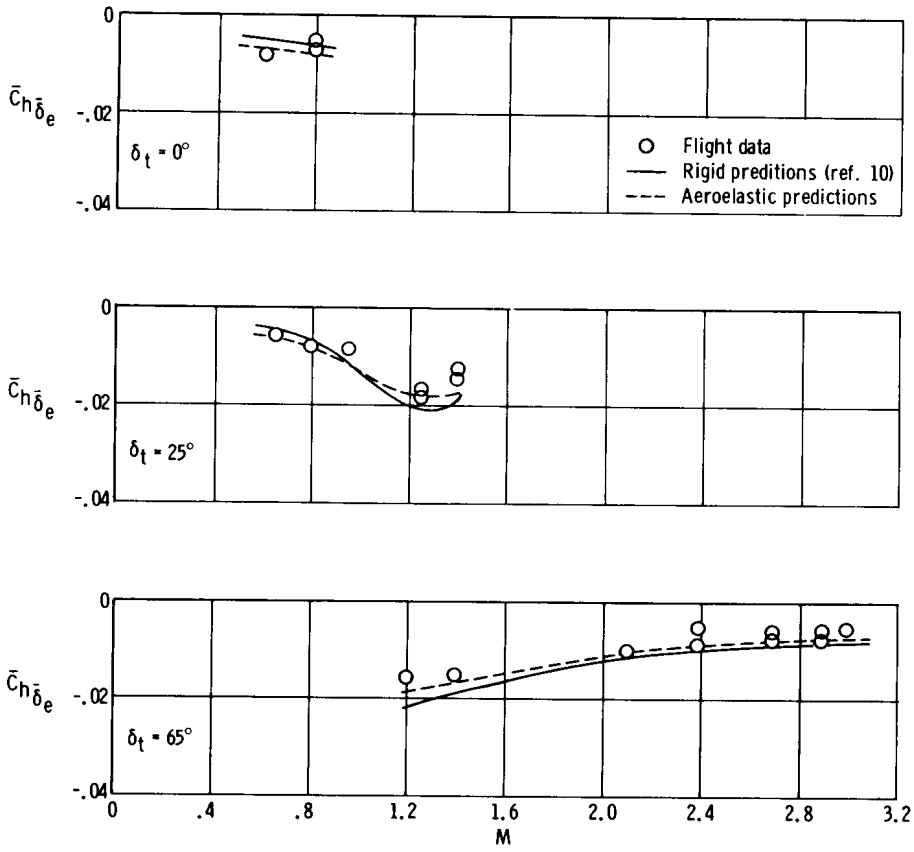

Figure 16.– Comparison of the average elevon hinge-moment-coefficient slopes with predicted values at various Mach numbers.

predicted. The slopes for the individual segments are presented in figure 17. No predictions are available for the individual segments.

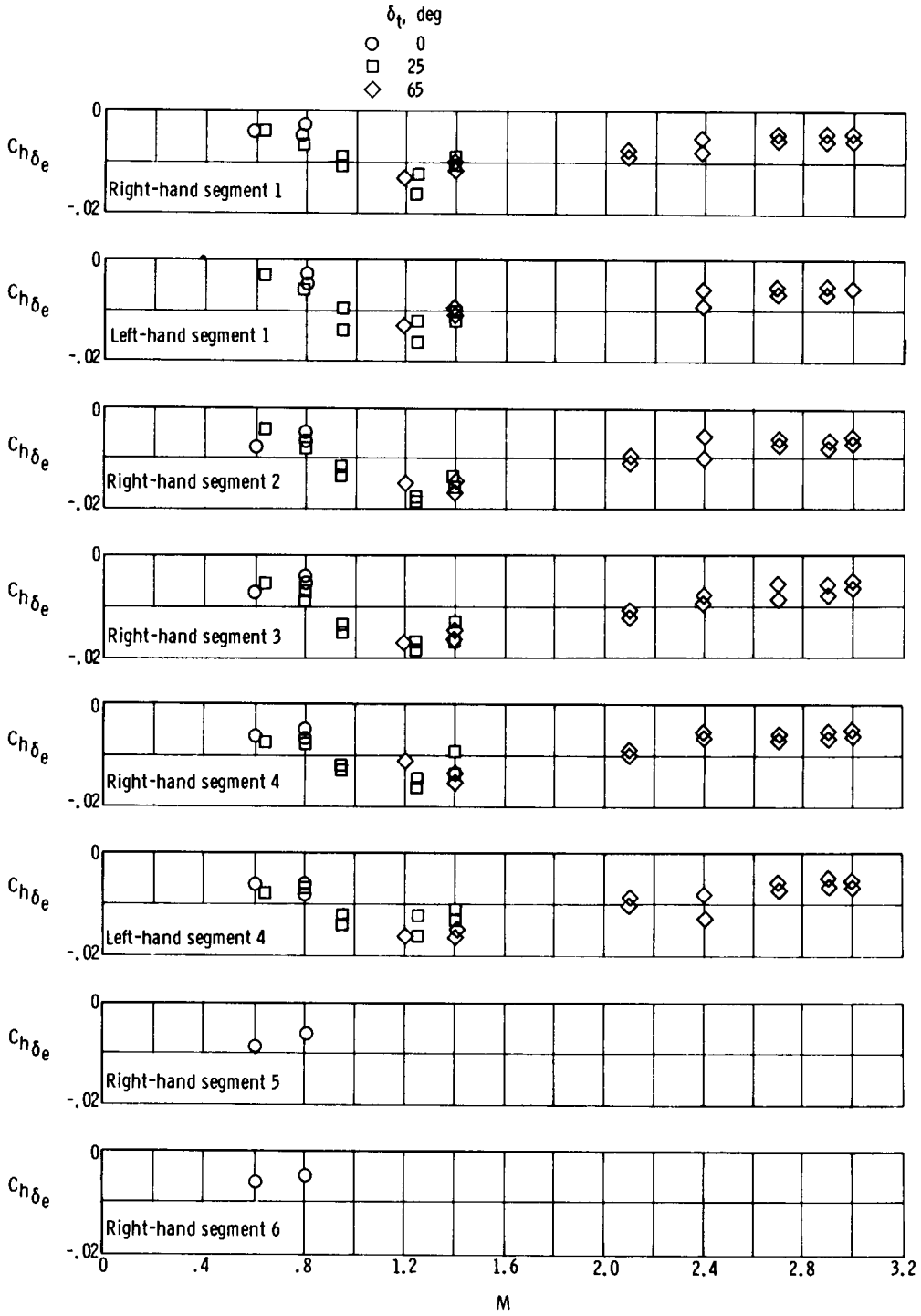

Figure 17.- Variation with Mach number of individual elevon-segment hinge-moment-coefficient slopes obtained from flight data.

Wing-Tip Hinge Moments

Wing-tip hinge-moment data were obtained on only the XB-70-2 airplane. These data are presented in figure 18 in the form of hinge-moment coefficients plotted against angle of attack for the three wing-tip positions at Mach numbers from 0.40 to 3.00.

Flight data are presented for the zero wing-tip deflection in figure 18(a) for the subsonic Mach numbers of 0.40 and 0.80. They are compared with wind-tunnel data obtained at Mach 0.60. The wind-tunnel data were obtained by integrating the rigid-model pressure-distribution data of reference 11. If it is assumed that the wind-tunnel data are linear between the two data points, then there is a slight difference in slope between the wind-tunnel data (M = 0.60) and the flight data at Mach 0.80. The flight data, in general, agree reasonably well with wind-tunnel data; however, the available range and extent of the data limit detailed conclusions concerning the correlation.

In figure 18(b) data are presented for the 25° wing-tip position. Flight data at Mach 0.80, 0.95, 1.25, and 1.40 are compared with the wind-tunnel data of reference 11, which were acquired at Mach 0.60, 0.95, and 1.20. The flight data at Mach 0.80 agree closely with the wind-tunnel data at Mach 0.60 for 8° angle of attack. Assuming a linear variation for the wind-tunnel data at Mach 0.95 between the two data points shown, the flight data at Mach 0.95 exhibit approximately the same slope, but are slightly lower in magnitude. The flight data at Mach 1.25 and 1.40 are slightly lower in magnitude than the wind-tunnel data at Mach 1.20 for 4° angle of attack. Although the amount of data available for specific comparison is limited, the general trend indicates the magnitude of the flight data to be either close to that of the wind-tunnel data or slightly lower.

Data are presented for the 65° wing-tip position in figure 18(c) for supersonic speeds. The flight data at Mach 1.20 and 1.40 are slightly lower in magnitude than the wind-tunnel data at Mach 1.20 for data near 4° angle of attack. The flight data at Mach 1.95 are slightly larger in magnitude than the wind-tunnel data at Mach 1.75 for data near 4° angle of attack. The flight data at Mach 2.80 and 3.00 agree closely with the wind-tunnel data at Mach 3.00 for data near 4° angle of attack.

If it is assumed that the wind-tunnel data are linear between the two points available, and considering that the range of variation of angle of attack for the flight data is limited, there is a general indication that the slope of the wing-tip hinge-moment coefficient—angle-of-attack variation of the flight data corresponds closely to that of the wind-tunnel data for supersonic flight. The limited data available for comparison at subsonic and transonic speeds indicate some differences in slopes between flight and wind-tunnel data.

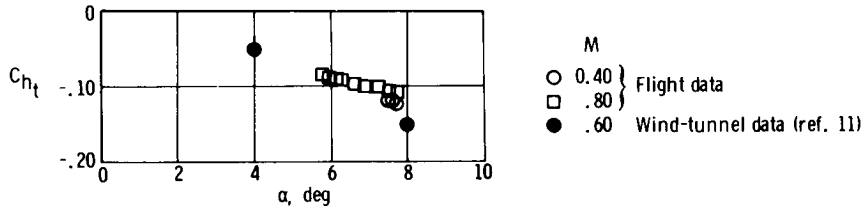

(a) $\delta_t = 0^o$.

Figure 18.– Comparison of wing-tip hinge-moment-coefficient measurements with wind-tunnel data for three wing-tip positions.

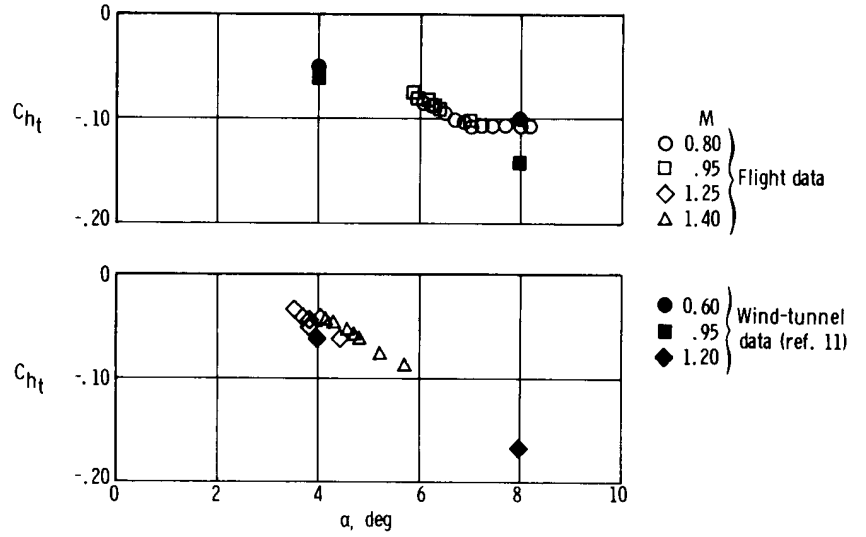

(b) $\delta_t = 25^o$.

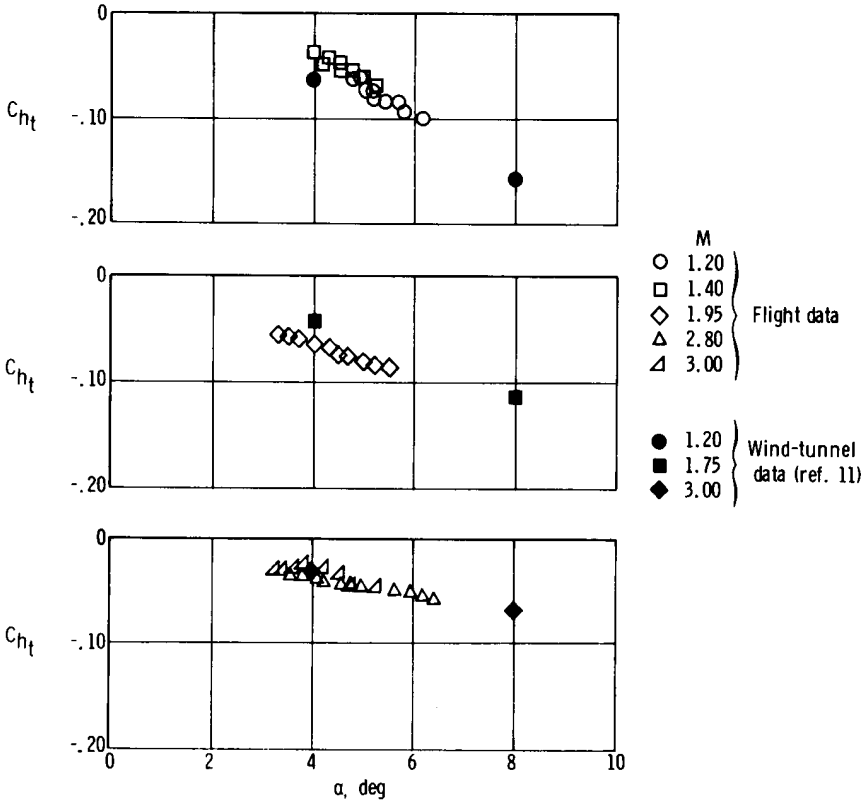

(c) $\delta_t = 65^o$.

Figure 18.– Concluded.

CONCLUDING REMARKS

Canard loads, elevon hinge moments, and wing-tip hinge moments measured in a flight-test program with the XB-70 airplane were compared with predicted values, wind-tunnel data, and results from flight tests of comparable airplanes. The general correlation of canard normal-force data with rigid and aeroelastic predictions indicated no significant variations from predicted results except in the transonic region. The canard-panel spanwise center of pressure agreed closely with predictions at subsonic speeds but was somewhat inboard of predictions at transonic and low supersonic speeds. The location of the canard-panel chordwise center of pressure was slightly aft of predictions at supersonic speeds, close to predictions at subsonic speeds, and aft of predictions at transonic speeds. The variation of canard-panel normal-force coefficient with canard angle-of-attack data compared reasonably well with predicted values, except in the transonic region, and with results obtained from other aircraft having wing—fuselage planforms similar to the XB-70 canard—fuselage planform.

Significant canard buffeting encountered at subsonic speeds was found to be caused by a leading-edge flow separation. The separation was most pronounced subsonically and abated as the transonic region was approached and penetrated. Root-mean-square bending-moment data revealed that, although significant buffeting of the canard panel was occurring, there was no appreciable corresponding loss of lift in the range of angle of attack investigated. The spanwise center of pressure moved inboard and the chordwise center of pressure moved aft as the angle of attack (and, correspondingly, the buffet intensity) increased. Power-spectral-density analyses of the canard root-mean-square unsteady-bending-moment data indicated the primary power to be canard first bending moment at approximately 9 cycles per second.

The elevon hinge-moment-coefficient flight data agreed generally well with predictions and wind-tunnel data. The most significant deviations were in and near the transonic region.

The wing-tip hinge-moment-coefficient data in general agreed well with the limited wind-tunnel data available for comparison.

Flight Research Center,
National Aeronautics and Space Administration,
Edwards, Calif., May 6, 1969.

REFERENCES

1. Andrews, William H.: Summary of Preliminary Data Derived From the XB-70 Airplanes. NASA TM X-1240, 1966.

2. Wilson, Ronald J.; and Larson, Richard R.: Statistical Analysis of Landing-Contact Conditions for the XB-70 Airplane. NASA TN D-4007, 1967.

3. Kordes, Eldon E.; and Love, Betty J.: Preliminary Evaluation of XB-70 Airplane Encounters With High-Altitude Turbulence. NASA TN D-4209, 1967.

4. Lasagna, Paul L.; and McLeod, Norman J.: Preliminary Measured and Predicted XB-70 Engine Noise. NASA TM X-1565, 1968.

5. Powers, Bruce G.: A Review of Transport Handling-Qualities Criteria in Terms of Preliminary XB-70 Flight Experience. NASA TM X-1584, 1967.

6. Wolowicz, Chester H.; Strutz, Larry W.; Gilyard, Glenn B.; and Matheny, Neil W.: Preliminary Flight Evaluation of the Stability and Control Derivatives and Dynamic Characteristics of the Unaugmented XB-70-1 Airplane Including Comparisons With Predictions. NASA TN D-4578, 1968.

7. Saltzman, Edwin J.; Goecke, Sheryll A.; and Pembo, Chris: Base Pressure Measurements on the XB-70 Airplane at Mach Numbers From 0.4 to 3.0. NASA TM X-1612, 1968.

8. Mechtly, E. A.: The International System of Units - Physical Constants and Conversion Factors. NASA SP-7012, 1964.

9. Skopinski, T. H.; Aiken, William S., Jr.; and Huston, Wilber B.: Calibration of Strain-Gage Installations in Aircraft Structures for the Measurement of Flight Loads. NACA Rept. 1178, 1954.

10. Aerodynamics Group: Aerodynamic Characteristics for Structural Analysis. XB-70 Air Vehicles #1 and 2. Vols. I and II. Rep. No. NA-64-973, North American Aviation, Inc., Oct. 1, 1964.

11. Wind Tunnel Projects: Trisonic Wind Tunnel Tests of an .03 Scale XB-70 Pressure Model to Determine Pressure Distribution at Mach Numbers .60 to 3.0. Vols. I-IV. Rep. No. NA-62-1275, North American Aviation, Inc., Oct. 1, 1962.

12. Hedstrom, C. Ernest; and Green, Kendal H.: Static-Stability and Control Characteristics and Control Surface Hinge Moments of a 0.03-Scale Model of the XB-70 Airplane at Supersonic Speeds. NASA TM X-1410, 1967.

13. Keener, Earl R.; and Jordan, Gareth H.: Wing Loads and Load Distributions Throughout the Lift Range of the Douglas X-3 Research Airplane at Transonic Speeds. NACA RM H56G13, 1956.

14. Pyle, Jon S.: Flight-Measured Wing Surface Pressures and Loads for the X-15 Airplane at Mach Numbers From 1.2 to 6.0. NASA TN D-2602, 1965.

15. Huston, Wilber B.; Rainey, A. Gerald; and Baker, Thomas F.: A Study of the Correlation Between Flight and Wind-Tunnel Buffeting Loads. NACA RM L55E16b, 1955.

16. Huston, Wilber B.; and Skopinski, T. H.: Measurement and Analysis of Wing and Tail Buffeting Loads on a Fighter Airplane. NACA Rept. 1219, 1955. (Supersedes NACA TN 3080.)

17. Baker, Thomas F.; Martin, James A.; and Scott, Betty J.: Flight Data Pertinent to Buffeting and Maximum Normal-Force Coefficient of the Douglas X-3 Research Airplane. NACA RM H57H09, 1957.

18. Coe, Charles F.; and Mellenthin, Jack A.: Buffeting Forces on Two-Dimensional Airfoils as Affected by Thickness and Thickness Distribution. NACA RM A53K24, 1954.

TABLE I. – GEOMETRIC CHARACTERISTICS OF THE XB-70-1 AIRPLANE

Wing –	
Total area, includes 2482.34 ft^2 (230.62 m^2) covered by fuselage but not 33.53 ft^2 (3.12 m^2) of the wing ramp area, ft^2 (m^2)	6297.8 (585.07)
Span, ft (m)	105 (32)
Aspect ratio	1.751
Taper ratio	0.019
Dihedral angle, deg	0
Root chord (wing station 0), ft (m)	117.76 (35.89)
Tip chord (wing station 630 in. (16 m)), ft (m)	2.19 (0.67)
Mean aerodynamic chord, in. (m):	942.38 (23.94)
Wing station, in. (m)	213.85 (5.43)
Fuselage station of 25-percent wing mean aerodynamic chord, in. (m)	1621.22 (41.18)
Sweepback angle, deg:	
Leading edge	65.57
25-percent element	58.79
Trailing edge	0
Airfoil section	0.30 to 0.70 HEX (MOD)
Thickness, percent chord:	
Wing station -	
Root to 186 in. (4.72 m)	2.0
460 in. to 630 in. (11.68 m to 16 m)	2.5
Folding wing tip (data for one tip only) –	
Area, ft^2 (m^2)	520.90 (48.39)
Span, ft (m)	20.78 (6.33)
Aspect ratio	0.829
Taper ratio	0.046
Root chord, wing station 380.62 in. (9.67 m), ft (m)	47.94 (14.61)
Tip chord, wing station 630 in. (16 m), ft (m)	2.19 (0.67)
Mean aerodynamic chord (wing station 467.37 in. (11.87 m)), in. (m)	384.25 (9.76)
Down deflection from inboard wing, deg	0, 25, 65
Elevons (data for one side) –	
Total effective area aft of hinge line, includes 3.33 ft^2 (0.31 m^2) air gap at wing-tip fold line, ft^2 (m^2)	197.7 (18.37)
Span, ft (m):	
Wing tips up	20.44 (6.23)
Wing tips down	13.98 (4.26)
Chord, in. (m)	116 (2.95)
Sweepback of hinge line, deg	0
Canard –	
Area, includes 150.31 ft^2 (13.96 m^2) covered by fuselage, ft^2 (m^2)	415.59 (38.61)
Span, ft (m)	28.81 (8.78)
Aspect ratio	1.997
Taper ratio	0.388
Dihedral angle, deg	0
Root chord (canard station 0), ft (m)	20.79 (6.34)
Tip chord (canard station 172.86 in. (4.39 m)), ft (m)	8.06 (2.46)
Mean aerodynamic chord, in. (m):	184.3 (4.68)
Canard station, in. (m)	73.71 (1.87)
Fuselage station of 25-percent chord, in. (m)	553.73 (14.06)
Sweepback angle, deg:	
Leading edge	31.70
25-percent element	21.64
Trailing edge	-14.91

TABLE I. – GEOMETRIC CHARACTERISTICS OF THE XB-70-1 AIRPLANE - Concluded

Airfoil section	0.34 to 0.66 HEX (MOD)
Thickness chord ratio, percent:	
Root	2.5
Tip	2.52
Ratio of canard area to wing area	0.066
Canard flap (data for one side) –	
Area (aft of hinge line), ft^2 (m^2)	54.69 (5.08)
Inboard chord canard station 47.93 in. (1.22 m), ft (m)	7.16 (2.18)
Outboard chord canard station 172.86 in. (4.39 m), ft (m)	3.34 (1.02)
Ratio of flap area to canard semiarea	0.263
Vertical tail (one of two) –	
Area (includes 8.96 ft^2 (0.83 m^2) blanketed area), ft^2 (m^2)	233.96 (21.74)
Span, ft (m)	15 (4.57)
Aspect ratio	1
Root chord (vertical-tail station 0), ft (m):	23.08 (7.03)
Tip chord (vertical-tail station 180 in. (4.57 m)), ft (m)	6.92 (2.11)
Taper ratio	0.30
Mean aerodynamic chord, in. (m):	197.40 (5.01)
Vertical-tail station, in. (m)	73.85 (1.88)
Fuselage station of 25-percent chord	2188.50 (55.59)
Sweepback angle, deg:	
Leading edge	51.77
25-percent element	45
Trailing edge	10.89
Airfoil section	0.30 to 0.70 HEX (MOD)
Thickness chord ratio, percent:	
Root	3.75
Tip	2.50
Cant angle, deg	0
Ratio of vertical tail to wing area	0.037
Rudder –	
Area, includes 8.66 ft^2 (0.81 m^2) blanketed area, ft^2 (m^2)	191.11 (17.76)
Span, ft (m)	15.00 (4.57)
Root chord, vertical-tail station 0, ft (m)	9.16 (2.79)
Tip chord, vertical-tail station 180 in. (4.57 m), ft (m)	6.92 (2.11)
Sweepback of hinge line	-45.0
Ratio of rudder area to vertical-tail area	0.82
Fuselage (includes canopy) –	
Length, ft (m)	185.75 (56.62)
Maximum depth (fuselage station 878 in. (22.30 m)), in. (m)	106.92 (2.72)
Maximum breadth (fuselage station 855 in. (21.72 m)), in. (m)	100 (2.54)
Side area, ft^2 (m^2)	939.72 (87.30)
Planform area, ft^2 (m^2)	1184.78 (110.07)
Canard exposed panel (one side) –	
Area, ft^2 (m^2)	132.64 (12.32)
Span, ft (m)	10.46 (3.19)
Root chord (canard station 47.35 in. (1.20 m)), ft (m)	17.30 (5.27)
Tip chord (canard station 172.86 in. (4.39 m)), ft (m)	8.06 (2.46)
Mean aerodynamic chord, in. (m):	158.91 (4.04)
Canard station, in. (m)	132.47 (3.36)
Fuselage station of leading edge, in. (m)	525.42 (13.35)

TABLE II. – XB-70 FLIGHT CONDITIONS

Figure number	Wing-tip position, deg	Mach number	α, deg	Gross weight, lb (N)	Center of gravity, percent mean aerodynamic chord	Aircraft number - flight number	Maneuver	h_p, ft (m)	q, lb/ft^2 (N/m^2)
5 to 7	--	0.60	4.6 to 7.0	426,000 (1,895,000)	22.0	1-65	Push-over/pullup	12,000 (3,658)	350 (16,750)
5 to 7	--	.80	6.0 to 8.2	435,000 (1,935,000)	21.5	2-19	Windup turn	25,000 (7,620)	340 (16,280)
5 to 7	--	.95	5.7 to 7.5	463,000 (2,059,000)	21.9	2-19	Windup turn	30,000 (9,144)	385 (18,430)
5 to 7	--	1.20	4.9 to 6.4	345,000 (1,535,000)	23.4	2-19	Windup turn	40,000 (12,190)	370 (17,710)
5 to 7	--	1.40	4.1 to 5.8	395,000 (1,757,000)	20.8	2-19	Windup turn	40,000 (12,190)	525 (25,130)
5 to 7	--	2.10	5.5 to 6.8	305,000 (1,356,000)	23.4	2-15	Turn	65,000 (19,810)	375 (17,950)
5 to 7	--	2.60	3.6 to 5.9	365,000 (1,642,000)	21.3	2-13	Windup turn	60,000 (18,290)	660 (31,590)
5 to 7	--	2.80	4.5 to 6.9	Unknown	Unknown	2-14	Windup turn	70,000 (21,340)	575 (27,530)
5 to 7	--	3.00	3.4 to 4.0	315,000 (1,401,000)	19.19	2-18	Trim	70,000 (21,340)	630 (30,160)
9 to 13	--	.50	5.1 to 9.5	309,000 (1,374,000)	22.7	1-71	Pullup	16,200 (4,938)	200 (9,570)
9 to 13	--	.56	4.8 to 8.1	311,000 (1,383,000)	22.2	1-71	Pullup	16,700 (5,090)	248 (11,870)
9 to 13	--	.61	4.6 to 7.2	426,000 (1,895,000)	22.0	1-65	Pullup	11,900 (3,672)	360 (17,230)
9 to 13	--	.71	3.4 to 6.8	465,000 (2,068,000)	22.1	1-66	Pullup	15,000 (4,572)	420 (20,100)
9 to 13	--	.82	4.5 to 9.4	435,000 (1,935,000)	21.8	1-71	Pullup	32,200 (9,815)	267 (12,780)
9 to 13	--	.91	5.0 to 8.1	Unknown	Unknown	1-75	Pullup	35,500 (10,820)	282 (13,500)
14 to 21	0	.60	≈3	290,000 (1,290,000)	22.3	2-10	Windup turn	15,000 (4,572)	295 (14,120)
14 to 21	0	.80	≈6	445,000 (1,979,000)	22.1	2-19	Pullup	25,000 (7,620)	350 (16,750)
14 to 21	0	.80	≈7	440,000 (1,957,000)	21.9	2-19	Windup turn	25,000 (7,620)	360 (17,230)
14 to 21	25	.65	≈2	325,000 (1,446,000)	20.3	2-21	Trim	2,500 (762)	555 (26,560)
14 to 21	25	.65	≈3	325,000 (1,446,000)	20.3	2-21	Trim	2,500 (762)	555 (26,560)
14 to 21	25	.80	≈6	435,000 (1,935,000)	21.5	2-19	Windup turn	25,000 (7,620)	335 (16,040)
14 to 21	25	.80	≈7	435,000 (1,935,000)	21.5	2-19	Windup turn	25,000 (7,620)	335 (16,040)
14 to 21	25	.95	≈6	465,000 (2,068,000)	21.9	2-19	Windup turn	30,000 (9,144)	385 (18,430)
14 to 21	25	.95	≈7	465,000 (2,068,000)	21.9	2-19	Windup turn	30,000 (9,144)	385 (18,430)
14 to 21	25	1.25	≈4	290,000 (1,290,000)	22.9	2-19	Windup turn	40,000 (12,190)	400 (19,150) to 520 (24,890)
14 to 21	25	1.25	≈5	290,000 (1,290,000)	22.9	2-19	Windup turn	40,000 (12,190)	400 (19,150) to 520 (24,890)
14 to 21	25	1.40	≈4	395,000 (1,757,000)	20.8	2-19	Windup turn	40,000 (12,190)	525 (25,130)
14 to 21	25	1.40	≈5	395,000 (1,757,000)	20.8	2-19	Windup turn	40,000 (12,190)	525 (25,130)
14 to 21	65	1.20	≈6	345,000 (1,535,000)	23.4	2-19	Windup turn	40,000 (12,190)	375 (17,950)
14 to 21	65	1.40	≈4	375,000 (1,668,000)	19.9	2-19	Pullup	40,000 (12,190)	555 (26,570)
14 to 21	65	1.40	≈5	385,000 (1,712,000)	20.9	2-19	Windup turn	40,000 (12,190)	525 (25,130)
14 to 21	65	2.10	≈3	385,000 (1,712,000)	21.2	2-6	Windup turn	50,000 (15,240)	760 (36,380)
14 to 21	65	2.10	≈4	385,000 (1,712,000)	21.2	2-6	Windup turn	50,000 (15,240)	750 (35,900)
14 to 21	65	2.40	≈3	420,000 (1,868,000)	21.7	2-25	Pullup	55,000 (16,760)	700 (33,500)
14 to 21	65	2.40	≈4	420,000 (1,868,000)	21.7	2-25	Pullup	55,000 (16,760)	700 (33,500)
14 to 21	65	2.90	≈4	320,000 (1,423,000)	23.8	2-26	Pullup	70,000 (21,340)	540 (25,850)
14 to 21	65	2.90	≈5	310,000 (1,379,000)	23.8	2-26	Windup turn	70,000 (21,340)	540 (25,850)
14 to 21	65	2.90	≈6	310,000 (1,379,000)	23.8	2-26	Windup turn	70,000 (21,340)	530 (25,370)
14 to 21	65	2.90	≈7	310,000 (1,379,000)	23.8	2-26	Windup turn	70,000 (21,340)	525 (25,130)
14 to 21	65	3.00	≈4	330,000 (1,468,000)	21.0	2-20	Pullup	70,000 (21,340)	580 (27,760)
14 to 21	65	3.00	≈5	330,000 (1,468,000)	21.2	2-20	Pullup	70,000 (21,340)	595 (28,480)
14 to 21	65	3.00	≈6	330,000 (1,468,000)	21.0	2-20	Pullup	70,000 (21,340)	605 (28,960)